Journal of Hydrology 645 (2024) 132268

Contents lists available at ScienceDirect

Journal of Hydrology

journal homepage: www.elsevier.com/locate/jhydrol

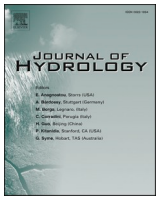

Research papers

Sensitivity of mass flux reduction and mass removal of perfluoroalkyl substances to groundwater flow and transport parameter variability and heterogeneity

Ruba A.M. Mohamed [a], Mohamad R. Soltanian [b], Dengjun Wang [c], Kenneth C. Carroll [a,*]

[a] Department of Plant and Environmental Sciences, New Mexico State University, Las Cruces, NM, 88003, USA
[b] Department of Geosciences & Department of Environmental Engineering, University of Cincinnati, Cincinnati, OH, 45221, USA
[c] School of Fisheries, Aquaculture and Aquatic Sciences, Auburn University, Auburn, AL, 36849, USA

ARTICLE INFO

Keywords:
PFAS
Heterogeneity
Transport
Model sensitivity
Mass flux reduction
Mass removal

ABSTRACT

Heterogeneity of soil hydraulic (e.g., hydraulic conductivity (K_S), porosity (θ_S)) and chemical (e.g., solid-phase adsorption (K_d)) properties complicates contaminant transport by creating spatial variability in sources of contaminant leaching. There is a knowledge gap on the effect of the interplay between these properties on the retardation and transport of per- and polyfluoroalkyl substances (PFAS) with different properties including carbon–fluorine chain-length and functional groups even in water-saturated conditions. Breakthrough curves have been used to evaluate PFAS transport behavior through heterogeneous media, including arrival time, maximum concentration, and tailing behavior. Contaminant mass flux reduction and mass removal correlations are also compared using numerical modeling to characterize PFAS transport through different source zones within a two-domain, heterogeneous system with comparison to homogeneous scenarios under water-saturated conditions. With heterogeneous properties, model sensitivity to K_S was the highest among the other parameters and was controlled by the K_S ratio between the different soils. The PFAS models in the homogeneous and heterogeneous scenarios were both sensitive to θ_S, depending on PFAS chain length. However, long-chain PFAS were less sensitive to θ_S variability compared to short-chain PFAS due to their higher K_d. The homogeneous and heterogeneous scenarios were equally sensitive to K_d variability, which was dependent on PFAS chain length.

1. Introduction

Per – and polyfluoroalkyl substances (PFAS) are synthetic, fluorinated organic compounds created in the 1940s that have been used as stain, oil, and water repellants (Glüge et al., 2020; Johnson et al., 2022). Some of the main sources of PFAS in the environment include aqueous film forming foams (AFFF), biosolid landfill applications, and effluents from wastewater treatment plants, which contributed to global contamination of surface water, soils, and groundwater (Bolan et al., 2021; Dasu et al., 2022; Hu et al., 2016; Johnson et al., 2022; Kurwadkar et al., 2022; McGarr et al., 2023). Due to the strong carbon–fluorine bonds, PFAS are considered persistent and recalcitrant in the environment and several PFAS species have been found to be harmful to humans and animals (Cara et al., 2022; Ghisi et al., 2019; Peritore et al., 2023; Teunen et al., 2021; Vorst et al., 2021). The prolonged deposition of PFAS in the environment has raised concerns about their transport and retention in soils and aquifers, which urges investigation of effective removal strategies.

The transport and retention of PFAS in the vadose zone varies depending on the properties of the specific PFAS compound and soil properties (Brusseau, 2021; Brusseau et al., 2019a; Costanza et al., 2019; Huang et al., 2022; Sharifan et al., 2021; Silva et al., 2021). While PFAS share some general properties, their persistence level is closely related to their chemical structures and chain lengths. Long-chain PFAS, with eight or more carbon–fluorine bonds, are generally more hydrophobic compared to short-chain PFAS, leading to stronger interactions with soil organic matter (Brusseau, 2023; Gagliano et al., 2020; Kookana et al., 2022; Makselon, 2019). The two main subclasses of PFAS (carboxylic acid and sulfonic acid) exhibit different adsorption affinities and retention behaviors within soils (Ahrens et al., 2010; Fabregat-Palau et al., 2021; Higgins and Luthy, 2006). Sulfonic acids, as stronger acids, readily donate protons to water and were found to have stronger

* Corresponding author at: Department of Plant and Environmental Sciences, New Mexico State University, P. O. Box 30003, Las Cruces, NM, 88003, USA.
E-mail address: kccarr@nmsu.edu (K.C. Carroll).

https://doi.org/10.1016/j.jhydrol.2024.132268
Received 20 May 2024; Received in revised form 10 October 2024; Accepted 14 October 2024
Available online 29 October 2024

adsorption to sediments and suspended particles for the same pH and solute ionic strength (Higgins and Luthy, 2006; Huang et al., 2022; Nguyen et al., 2020; Pereira et al., 2018). Higgins and Luthy (2006) found that the partitioning coefficients of the perfluoroalkyl sulfonic acids were 0.23 log units higher compared to the perfluoroalkyl carboxylic acids with the same carbon chain length. Additionally, adsorption of PFAS to air–water and oil–water interfaces can be a significant retention process under unsaturated soil conditions in the vadose zone (Guo and Brusseau, 2024). Long-chain PFAS have been observed to have higher affinity to adsorb at fluid–fluid interfaces, particularly at higher solute concentrations (Brusseau, 2019; Zeng et al., 2021). Zeng et al. (2021) found that PFAS transport models of vadose zone soils were more sensitive to interface properties for longer-chain PFAS, whereas short-chain PFAS were more influenced by solid-phase adsorption properties. Soil physical and chemical properties including soil texture, organic matter content, aquifer hydraulic conductivity (K_S), porosity (θ_S), pH, moisture content, ionic strength, and redox conditions play crucial roles in PFAS retention (Brusseau et al., 2019b; Van Glubt et al., 2021; Wang et al., 2021a).

The complex interplay of these factors in heterogeneous aquifers with variable physical and chemical properties makes it challenging to predict and manage PFAS retention in soil (Hitzelberger et al., 2022). In water-saturated, heterogeneous aquifers where the air–water interface is negligible, PFAS retention is controlled by variable nonlinear adsorption, kinetic adsorption, and hydraulic properties of soils, which can be spatially variable and result in development of secondary source zones (Hitzelberger et al., 2022). The solid-phase adsorption partitioning coefficient (K_d) may correlate positively or negatively with K_S and θ_S depending on the type of soil and solute chemical properties (Cvetkovic and Dagan, 1994; Cvetkovic and Shapiro, 1990; Dagan, 1984; Michael and Khan, 2016; Soltanian and Ritzi, 2014; Talon et al., 2023; Van der Zee and Van Riemsdijk, 1987). In turn, the correlation can be negative or positive depending on sediment type and the solute chemistry (Soltanian and Ritzi, 2014). A model with negative correlation between K_d and K_S is most often used for sedimentary sandy-clayey rocks (Allen-King et al., 1998; Allen-King et al., 2015; Soltanian et al., 2015b; Soltanian et al., 2015c; Tompson, 1993). Increasing clay content is generally positively correlated with K_d along with decreases in K_s, because the latter is related to permeability, which is inversely related to clay content. In contrast, a different pattern can be observed in fractured crystalline rocks (Chen et al., 2023; Dai et al., 2012; Soltanian et al., 2015a). Physical and chemical weathering causes the disintegration of rocks, and leads to the formation of weathering products (void coating and/or filling material), which tends to increase the amount of sorption reactive sites. Similarly, fracture aperture tends to increase resulting in an increase in both K_d and K_s. Thus, the positive correlation between the two characteristics is also possible. In some cases, examples that contradict this phenomenon were found in the literature where the presence of a small amount of reactive solid surfaces may dominate the sorption behavior but have little effect on the hydraulic conductivity both in sedimentary and crystalline rock systems (Dai et al., 2009; Zhao et al., 2005).

Regression between mass flux reduction (MFR) and mass removal (MR) in contaminant mass flux has been developed as a method for characterizing contamination sources and remediation of contaminants in heterogeneous porous media (Goltz et al., 2007; Soga et al., 2004). Both MFR and MR are critical metrics for evaluating the performance of groundwater remediation systems, such as pump-and-treat, in-situ chemical treatment, and natural attenuation processes (Brusseau et al., 2011; Difilippo and Brusseau, 2008; DiFilippo and Brusseau, 2011a; DiFilippo and Brusseau, 2011b; DiFilippo et al., 2010; Jawitz et al., 2008; Lemke et al., 2004; Marble et al., 2014; Marble et al., 2008; Mateas et al., 2017; Soga et al., 2007; Soga et al., 2004; Zareitalabad et al., 2013). A higher MFR value indicates a more effective remediation system. Achieving a high MFR to MR ratio is often a primary goal in contaminated aquifer remediation to minimize the impact of contaminants on the environment and human health. These metrics are also used to track the progress of remediation efforts over time and adjust the treatment strategy, if necessary. MFR-MR curves have been used to evaluate cleanup methods for organic liquid spills of nonaqueous phase liquid (NAPL) contamination in various types of source zones (Akyol et al., 2023; Slavic, 2014). Quantification of MFR and MR is crucial for designing in-situ stabilization or flushing cleanup methods for contaminants.

Recent efforts have characterized transport of PFAS in soils and aquifers with consideration of PFAS partitioning between solids, air, and liquid interfaces (Brusseau et al., 2019a; Brusseau et al., 2019b; Wang et al., 2021b; Zeng et al., 2021; Zeng and Guo, 2021). Recent work has investigated the effect of multiple hydrogeophysical properties and examined the effect of soil heterogeneity on PFAS retention and the development of preferential pathways for flow and transport under water-saturated conditions (Hitzelberger et al., 2022). Under unsaturated or variably saturated water flow, Guo et al. (2020) developed a mathematical model to represent PFAS-specific transport processes including surfactant-induced flow (SIF), non-linear and rate-limited solid-phase adsorption (SPA), and air–water interfacial adsorption (AWIA). Other work on unsaturated transport has demonstrated the differences in PFAS adsorption and chemical equilibrium at air–water interfaces for the bulk capillary water and thin-water-film, influenced by the different solid surface forces including electrostatic and Van der Waals forces (Zhang & Guo, 2024). Silva et al. (2020) modified HYDRUS unsaturated flow and transport model to simulate the effects of non-linear AWIA, solution surface tension-induced flow, and variable solution viscosity on PFAS transport within the unsaturated vadose zone. Their findings demonstrated that soil heterogeneities significantly influence the long-term leaching of the long-chain PFAS more than that of their short-chain counterparts. Another study by Maghrebi et al. (2015) found that the simulated breakthrough curve (BTC) concentration tailing was very sensitive to the vertical extent of the thin layers of lower-*Ks* materials, with longer tailing generated by the thicker lower-*Ks* materials. They also noted that K_d was more important for the lower-*Ks* material as it affected the tailing in the BTC, and the simulated BTC tailing was sensitive to the volume fraction of thin, lower-*Ks* facies. The sensitivity depended on the shape of these facies; however, the impact of volume fractions on tailing was found to be smaller than the impact of shape (i.e., thickness of thin lower-*Ks* facies). The results indicated that highly-sorbing, sandy-gravel material, with higher-*Ks*, can cause plume delays. Further research is needed to examine these sorption assumptions since, for example, non-linearity in sorption isotherms can produce different behaviors including nonideal contaminant transport with low concentration tailing during elution.

The objective of this research is to develop and compare BTC and MFR/MR correlations for transport of various PFAS compounds in two different domains (i.e., homogeneous and heterogeneous) under water-saturated conditions and to assess the BTC and MFR/MR curve sensitivity to variable flow and transport parameters. Numerical models were created to simulate solute transport of individual solutes for a wide variety of PFAS, with different chain-lengths and functional groups (i.e., carboxylic and sulfonic acids). The PFAS investigated include perfluorobutane sulfonate (PFBS), perfluoropentanoic acid (PFPeA), perfluoro-hexanesulfonic acid (PFHxS), perfluorooctanoic acid (PFOA), and perfluorooctanesulfonic acid (PFOS). The results were used to create BTCs and MFR/MR curves for several commonly encountered PFAS contaminants. To our knowledge, this is the first examination of solute transport parameter sensitivity or variability for various PFAS in both homogeneous and heterogeneous systems including analysis of sensitivity or variability of MFR/MR behavior. MFR/MR correlation and regression curves quantify the mass flow rate of PFAS exiting or eluting an aquifer naturally or through remediation. MFR-MR curves can help in either predicting natural contaminant release or to assist with optimizing the operation of remediation systems by identifying trends and patterns in contaminant mass removal. This insight allows engineers to

adjust remediation parameters such as flow rates, extraction well locations, or treatment processes based on the observed performance trends to enhance remediation efficiency.

2. Methods

2.1. Numerical model

HYDRUS (2D/3D) computer software package was used to numerically simulate water and solute transport in a two-dimensional model (Šimůnek et al., 2014; Šimůnek et al., 2016). Model domain was set as a rectangle (40.0 cm × 12.0 cm) with a 2.5 cm depth and is referred to in this paper as a 'flow cell' as analog for a portion of the subsurface. This study focused on parameters for two types of soils; F70 Ottawa sand (natural quartz sand with organic-carbon (0.04 %), metal-oxide (14 μg/g Fe, 12 ug/g Al, and 2.5 μg/g Mn), and clay mineral 89 % contents) and Vinton soil (sandy loam, mixed, thermic Typic Torrifluvent; consists of 54 % silica, 36 % feldspar, 3 % amphibole, and 4.7 % clay minerals, the clay minerals consist of similar proportions of kaolinite, vermiculite, and illite, with small fractions of montmorillonite and amorphous silica). It has (0.1 %) organic carbon content and a higher metal-oxide content than N70 Ottawa sand). The two soils have distinctively different K_S, θ_S, and K_d. Vinton has lower K_S, higher θ_S, and higher K_d for all PFAS compared to Ottawa sand. As a result, the insertion of Vinton within Ottawa sand altered the transport of PFAS through different mechanisms and the effect of the interplay between those mechanisms on the retention of these five PFAS and other PFAS remains largely unknown.

Model parameters were adapted from Zeng et al. (2021). Soil hydraulic parameters (K_S and θ_S) were determined independently by Karagunduz et al. (2015) (Table S1). The coefficient of variations of ln K_S and θ_S were estimated by Russo and Bouton (1992) as 0.26 and 0.056, respectively, and the values were used to determine the standard deviation given the average values (Table S2). The maximum and minimum K_S and θ_S were also estimated as mean + σ and mean − σ, respectively. The sorption partitioning coefficient was defined as:

$$K_d = K_f C^{N-1} \tag{1}$$

where C is the solute aqueous concentration (0.4 mg/L) which represents the average maximum concentration of all PFAS in a 1:100 diluted AFFF product. Using the same C value for all the models allows for a one-to-one comparison between the PFAS breakthrough and the retention times of the secondary source mass for all PFAS. The coefficients of variation for Freundlich SPA parameters, K_f (μmol/g) and N (−) were obtained from parameters measured by Van Glubt et al. (2021) as 0.12 and 0.05, respectively. K_f and N for PFOS in Ottawa sand and Vinton and for PFOA in Ottawa sand were adopted from previous studies (Brusseau, 2020; Guo et al., 2020; Van Glubt et al., 2021). Zeng et al. (2021) assumed that N values for the PFAS in each function group (carboxylic acid or sulfonic acid groups) were similar for each soil based on the previous rationale that nonlinearity for solid-phase adsorption is weak for a wide range of sediments (Guelfo and Higgins, 2013; Higgins and Luthy, 2006). K_f values for PFBS, PFPeA, and PFHxS were estimated by scaling K_f for PFOS and PFOA based on the organic carbon-normalized distribution coefficients reported in Zeng et al. (2021) (Table S3). The delta method was then used to approximate the variance of K_d given the variances of K_f and N (Supplementary S2). The delta method computes the asymptotic variance and confidence intervals for a non-linear function of a set of previously estimated parameters, typically by the method of maximum likelihood (Cox, 2005). The aqueous diffusion coefficients (D_0) of the PFAS were measured by Schaefer et al. (2019) (Table S4). The first-order rate constants for the kinetic solid-phase adsorption (α_s) were only available for PFOA and were estimated for the other PFAS compounds assuming that the first-order rate constants scaled with the molecular diffusion coefficients (Table S5). The bulk densities ρ_b exhibit a narrow range from field measurement and were assumed constants as 1.65 g/cm^3 for Ottawa sand and 1.624 g/cm^3 for Vinton (Zeng et al., 2021). The five PFAS modeled here include perfluorobutane sulfonate (PFBS; C4), perfluoropentanoic acid (PFPeA; C5), perfluorohexanesulfonic acid (PFHxS; C6),perfluorooctanoic acid (PFOA; C8), and perfluorooctanesulfonic acid (PFOS; C8).

Model configuration was based on the design used in various flow cell experiments and modeling publications that compared homogeneous conditions to heterogenous conditions that include two domains with an inclusion surrounded by a uniform matrix (e.g., Hitzelberger et al., 2022). The heterogeneous models consisted of a matrix of higher-permeability with one lenticular zone of lower-permeability material, which was shaped as a rectangular lens at the center of the flow cell (Fig. 1a). The homogeneous models contained only the higher-permeability matrix material. For the homogeneous models the domain was comprised of only one soil throughout the domain without spatial variability (Ottawa sand or Vinton), and for the heterogeneous models, the two soils combined (i.e., spatial variability) domain was comprised of a Vinton lens inclusion (12.0 cm × 4.0 cm) at the center of Ottawa sand (40.0 cm × 12.0 cm) (Fig. 1a). Models were conducted as a series of scenarios for each PFAS in each of the three different domains (i.e., homogeneous with Ottawa sand, homogeneous with Vinton, and heterogeneous).

Water and solute flow were set horizontally parallel to the long boundary of the modeled flow cell domain. Boundary conditions for the longer boundaries parallel to the flow direction were set as no flow/flux. The boundary conditions for the shorter-length, effluent boundary, configured perpendicular to the flow direction, were set as constant pressure head (h = 0), and the inflow boundary was set as a time variable flux. The initial conditions were set as h = 0 and C = 0. The solute with C = 0.4 mg/L was injected initially at a flow rate of 0.3 mL/min for 0.217 pore volume (PV), followed by a water flow rate of 0.2 mL/min (equivalent to an average pore water velocity of 9.6 cm/day) until the injected solute tracer was completely eluted. The two-dimensional advection–dispersion equation (ADE) is described as,

$$R\beta\frac{\partial c}{\partial t} = D_T\frac{\partial^2 c}{dx^2} + D_L\frac{\partial^2 c}{\partial z^2} - \nu\frac{\partial c}{\partial z} - \omega(C^* - S^*) \tag{2}$$

$$R = 1 + \frac{\rho}{\theta_S}K_d \tag{3}$$

$$\beta = \left(\frac{\theta_S + F_S\rho K_d}{\theta_S + \rho K_d}\right) \tag{4}$$

$$D_L = \alpha\nu + D_m \tag{5}$$

$$\omega = \left(\left(\frac{\alpha_S L}{\nu}\right)(1-\beta)R\right) \tag{6}$$

$$c^* = \frac{C}{C_0} \tag{7}$$

$$S^* = \left(\frac{1}{(1-F_S)K_d}\right)\left(\frac{S_2}{C_0}\right) \tag{8}$$

where C is the aqueous concentration, C_0 is the solute concentration in the input solution, R is the retardation factor, ρ is the bulk density, θ_s is the water-saturated porosity, K_d is the solid-phase adsorption coefficient, D_L and D_T are the longitudinal and transverse dispersion coefficients, respectively, D_m is the aqueous diffusion coefficient, and z and x are the spatial coordinates parallel and perpendicular to the direction of flow, ν is the average pore water velocity in the flow direction, C^* is the dimensionless solute concentration, L is the transport length, S_2 is the sorbed concentration in the rate-limited domain, S^* is the dimensionless sorbed concentration, α_S is the first-order sorption rate coefficient, F_S is the fraction of sorbent for which sorption is instantaneous, and β and ω are the dimensionless parameters that specify the

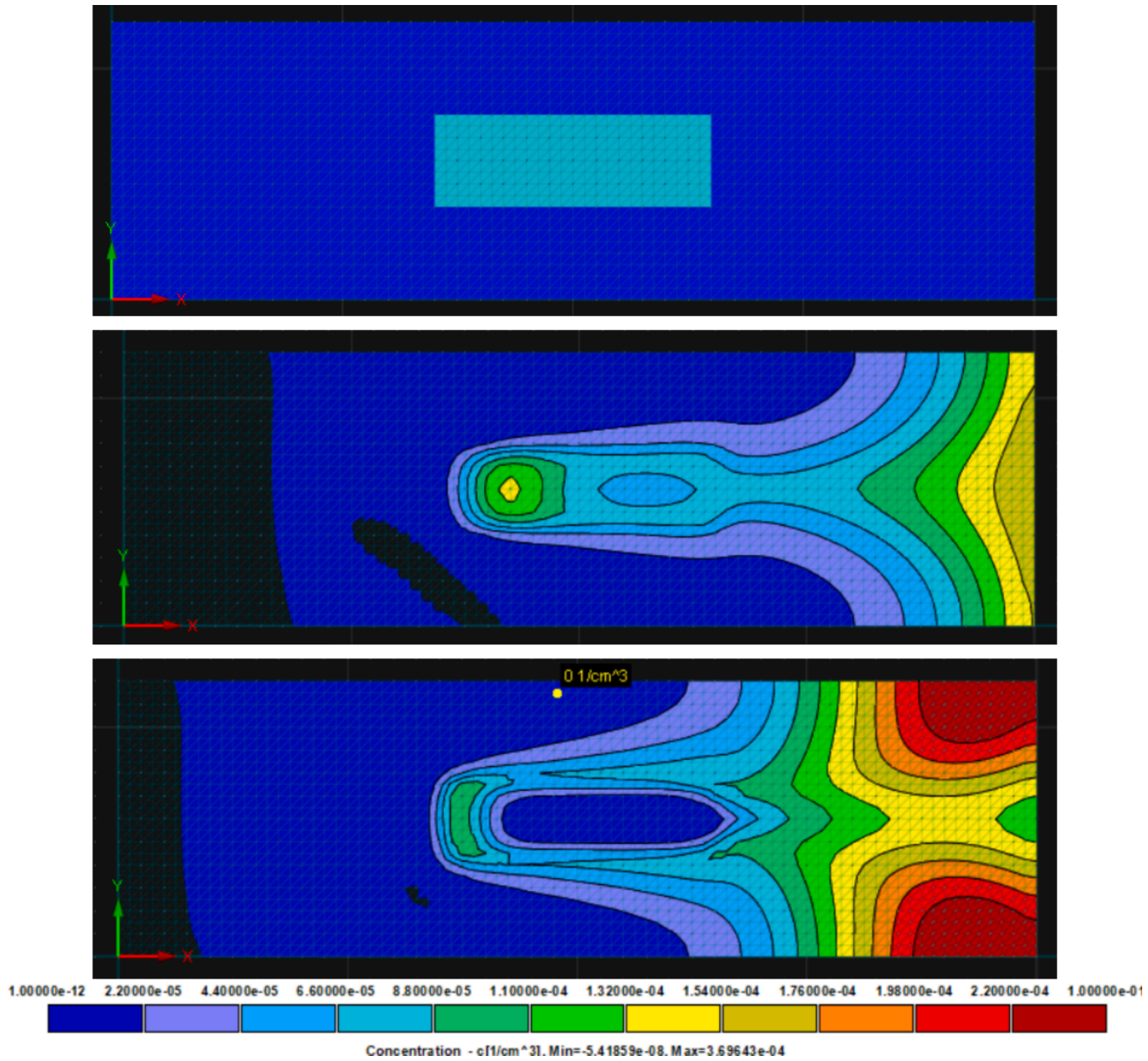

Fig. 1. (Top) The heterogeneous domain with Vinton lense at the center of Ottawa sand (Mesh size is 83 × 26 cm^2), (center) solute concentration countour of PFBS, and (bottom) solute concentration countour of PFOA at the beginning of mass removal.

degree of nonequilibrium in the system.

2.2. Sensitivity analysis

BTCs for the PFAS were constructed by plotting the solute effluent concentration in the liquid phase (C) normalized by the injected concentration (C_0) versus the pore volumes (PV) eluted, which is calculated as the injected volume normalized by the total porous volume. The product of the effluent concentration and flow rate was used to determine the transient mass discharge. Effluent concentrations and flow velocity were also used for moment analysis and mass balance calculations. Data points that occur after peak C/C_0 and end of solute tracer injection in the BTC data were used to create graphs of MFR versus MR as,

$$MFR = MR^n \tag{9}$$

$$1 - j_f/j_i = \left(1 - M_f/M_i\right)^n \tag{10}$$

where j_f is the final mass, j_i is the initial mass, n is a fitting parameter, M_f is the final source mass, and M_i is the initial source mass.

Three parameter statistics (i.e., mean, maximum (max), and minimum (min)) were used to construct models for the sensitivity analysis in the homogeneous domains (i.e., Ottawa sand and Vinton). The max and min statistics of each parameter were estimated using the mean and standard deviation values (i.e., max = mean + σ and min = mean – σ). For the homogeneous domains (i.e., Vinton and Ottawa sand), the three statistics (i.e., max, mean, and min) were used to create MFR/MR curves for each PFAS. For the heterogeneous domain, nine statistics were possible between the two soils for each parameter. MFR/MR curves were created for each of the three statistics per homogeneous domain and nine statistics in the heterogeneous domain.

The 'n' parameters were estimated by regression between log MFR

versus log MFR to examine the sensitivity of MFR/MR curves. The standard deviation of the 'n' parameter (σ_n) was estimated through regression to quantify MFR/MR sensitivity to the respective parameter variability. Sensitivity of the BTCs was quantified by the standard deviation of the elution PV (that led to zero C/C_0). Model sensitivity was evaluated through changes in the standard deviation of the elution PV obtained from the BTCs and the standard deviation of the 'n' parameter estimated by regression curve fitting. MFR-MR curves of the homogeneous domains followed a concave curve and therefore had one 'n' parameter value. MFR-MR curves of the heterogeneous domain followed a multi-step trend with a concave trend at an earlier stage of mass reduction and a convex trend at a later stage of mass reduction. Therefore, each MFR/MR curve of the heterogeneous domain had two 'n' parameters, with 'n1′ estimated for the lower-MR, concave portion of the curve and 'n2′ estimated for the higher-MR, convex portion of the curve. The inflection point between the concave and convex curves represents the completion of mass removal from the primary source and the beginning of mass removal from the secondary source, which is the less accessible zone in the two-domain system.

3. Results and discussion

The results have been organized as follows, 1) we examined and compared models results (i.e., BTCs and MFR-MR curves) for each of the five PFAS (i.e., PFBS, PFHxS, PFPeA, PFOA, and PFOS) in the homogeneous domain (in Ottawa sand and Vinton) and in the heterogeneous domain, using average parameters values. 2) Next, we quantified the sensitivity of the BTCs and MFR/MR curves to each of the three parameters (i.e., θ_s, K_s, and K_d) in the homogeneous and heterogeneous domains as described in section 2.2, 3) and then regressions were developed for the heterogeneous models between n1 versus parameter ratios (i.e., $\frac{K_s^{**}}{K_s}$, $\frac{\theta_s^{**}}{\theta_s}$, and $\frac{K_d^{**}}{K_d}$), n1 versus parameters area-weighted averages, elution PV versus parameters ratios, and elution PV versus the parameters area-weighted averages, to evaluate the controlling parameter statistics on the transport patterns and the trends of the BTCs and MFR/MR curves.

3.1. Model results using average parameters

The five PFAS examined in this study have different molecular weights, solid-phase adsorption K_d values, influenced by the PFAS chain-lengths and functional groups, and different kinetic adsorption coefficients (F_s and α_s) (Table S5). PFAS molecular weights affect their molecular diffusion, but this effect was found to be negligible in these advection–dispersion dominated fluid flow models. In this study, we examined the importance of kinetic adsorption by comparing BTCs of models with kinetic adsorption parameters F_s and α_s set to zero with comparison to models with the kinetic adsorption parameter values listed in Table S5, following the approach of Zeng et al. (2021). We found that the concentration retained through kinetic adsorption was more than two orders of magnitude less than the concentration retained by Freundlich solid-phase adsorption (Table S5).

Fig. 2 shows the BTCs and MFR-MR curves created from the transient models using the average parameters of θ_S, K_S, and K_d in homogeneous Ottawa sand, homogeneous Vinton, and heterogeneous domain. Vinton has K_d values that are one order of magnitude higher than Ottawa sand for all PFAS, which was reflected in about 0.3 – 0.7 times lower BTC C/C_0 peak in homogeneous Vinton compared to homogeneous Ottawa sand. Elution PV was also higher in Vinton and varied between 4.24 PV for PFBS to 10.3 PV for PFOS. Alternatively, elution PV in homogeneous Ottawa sand varied between 4.16 PV for PFBS to 5.32 PV for PFOS. Additionally, homogeneous Vinton has a lower average K_s (0.0702 cm/min) compared to homogeneous Ottawa sand (1.26 cm/min), which resulted in about 7.6 to 64.1 % increase in the peak arrival PV in homogeneous Vinton (Fig. 2a and b). K_d range in homogeneous Ottawa sand was within a standard deviation of 0.03 cm^3/g for all PFAS compared to a standard deviation of 0.15 cm^3/g in homogeneous Vinton, which resulted in higher variability in BTCs for transport in homogeneous Vinton (Fig. 2). The three short-chain PFAS had similar BTC C/C_0 in homogeneous Ottawa sand (0.7 ± 0.02) and similar elution PVs (0.28 ± 0.09), and the two long-chain PFAS had comparable BTC C/C_0 in homogeneous Ottawa sand (0.6 ± 0.01) and similar elution PV (5.28 ± 0.04). The MFR-MR curves of the two homogeneous soils followed concave trends for all PFAS and were aligned very closely (Fig. 2d and

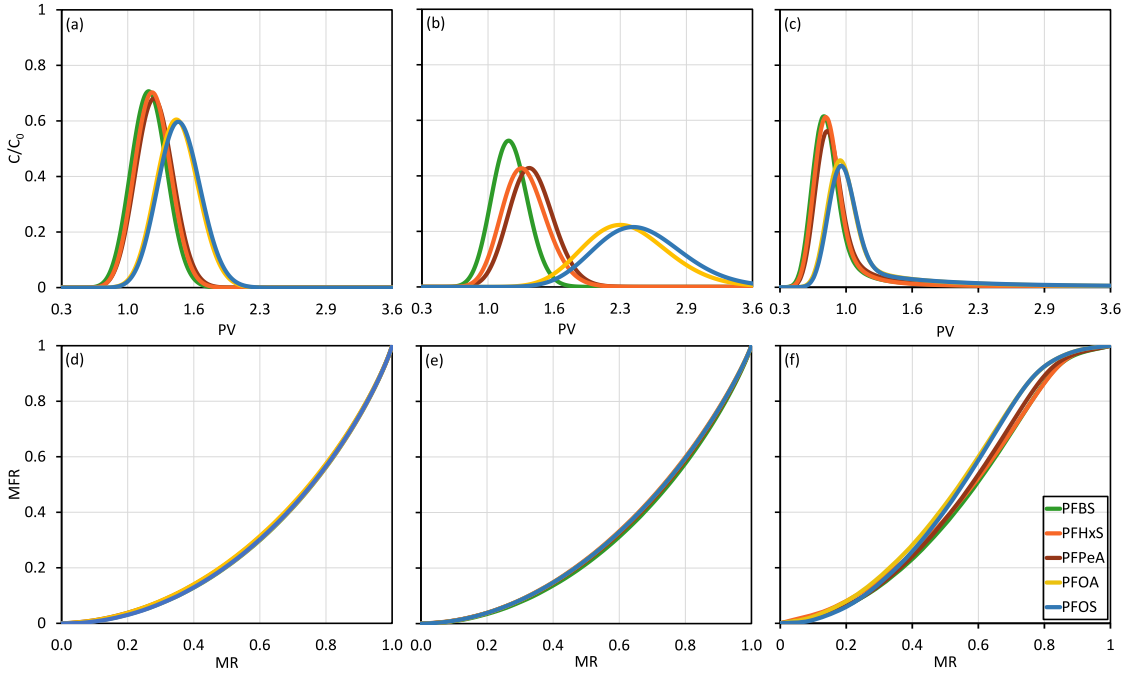

Fig. 2. Comparison of BTCs for the five PFAS in (a) homogeneous Ottawa sand, (b) homogeneous Vinton, and (c) heterogeneous flow cell domain, and MFR/MR curves of the five PFAS in (d) homogeneous Ottawa sand, (e) homogeneous Vinton, and (f) heterogeneous flow cell domain using the mean values for material properties.

e). The slope of the linear line that fits log MFR versus log MR (n1) for the homogeneous soils was used to quantify the sensitivity of the MFR/MR to the three parameters including K_S, θ_S, and K_d. Table S13 and S15) list n1 parameters for the homogeneous soils using three statistics (i.e., max, mean, and min) of each of the three parameters. When one of the statistics was used for one parameter, the mean values of the other two parameters were used in the model. n1 was greater than one for all PFAS in both homogeneous soils, indicating effective mass removal from the two homogeneous soils. The average n1 for all PFAS in homogeneous Ottawa sand was 2.08 ± 0.11, when the mean parameter values were used in the model, was similar to the average n1 in Vinton (2.02 ± 0.06). The n1 of the homogeneous soils does not seem to follow a pattern with PFAS chain length. These n1 statistics between homogeneous Vinton and homogeneous Ottawa sand indicates that MFR/MR are less sensitive to PFAS variability compared to BTCs and that may extend to other PFAS and different types of homogeneous soils.

The effect of domain heterogeneity and inclusion of Vinton as an inclusion lens in Ottawa sand was evaluated for the BTCs and MFR/MR curves of all PFAS (Fig. 2c and f). Peaks of all PFAS arrived at lower PV compared to the two homogeneous domains and all five PFAS eluted at larger PVs (Fig. 2c). The average PV for peak arrival for the three short-chain PFAS was 1.06 ± 0.02 compared to 1.19 ± 0.03 in homogeneous Ottawa sand and 1.26 ± 0.11 in homogeneous Vinton. The average PV for peak arrival for the two long-chain PFAS was 1.25 ± 0.003 compared to 1.44 ± 0.01 in homogeneous Ottawa sand and 2.32 ± 0.09 in homogeneous Vinton. Elution PVs also increased for each of the PFAS due to heterogeneity. PFAS had much higher average elution PVs in the heterogeneous domain (36.02 ± 3.91) compared to homogeneous Ottawa sand (4.28 ± 0.11) and homogeneous Vinton (5.04 ± 0.74), and the long-chain PFAS had much higher average elution PVs in the heterogeneous domain (73.56 ± 2.98) compared to homogeneous Ottawa sand (5.28 ± 0.06) and homogeneous Vinton (10.13 ± 0.25). Vinton has a lower K_S, higher θ_S, and higher K_d than Ottawa sand (Tables S1–S3). Higher K_S and higher θ_S generally increase the velocity and therefore accelerate the arrival of solutes, while higher K_d increases solutes retention and delays solutes elution. The inclusion of the Vinton lens within Ottawa sand created preferential flow paths, accelerating PFAS transport. Similar behavior was observed by Li et al. (2024), who demonstrated that in heterogeneous riparian sediments, high-permeability zones, such as sands and gravels, promote faster PFAS breakthrough and earlier plume arrival, despite varying sorption properties. Understanding the effect of heterogeneity and the interplay between the different parameters in the transport and retention of the different PFAS is crucial to predict the removal methods.

The MFR/MR curves of the heterogeneous domain followed a multi-step trend with a concave trend at a lower mass reduction (which represents the primary source zone with higher hydraulic accessibility), and a convex trend at the larger and later mass reduction portion of the curve (which represents the secondary mass source with the lower hydraulic accessibility) (Fig. 2f). This multi-step behavior was not observed in any of the homogeneous domain scenarios, and this multi-step behavior for heterogeneous domains is consistent with prior experimental and modeling research (DiFilippo, 2010; Hitzelberger et al., 2022). The parameter estimated by log MFR versus log MR regression of the concave trend was abbreviated as 'n1′ and the parameter estimated for the larger mass reduction, convex part of the trend was abbreviated as 'n2′. Tables S17 to S21 summarize n1, n2, and elution PVs for all PFAS transport through the heterogeneous domain from the nine parameter statistics combining Vinton and Ottawa sand parameters. The long-chain PFAS had a comparable mass flux reduction to the short-chain PFAS at the first stage of mass removal and up to 0.2 MR in the heterogeneous domain (Fig. 2f). At the first stage of MR, mass removed from the primary zone, which is more hydraulically accessible and has a small range of K_d for all PFAS. After 0.2 MR, mass reduction was higher for the short-chain PFAS, which indicated a more efficient mass removal.

Fig. 1 shows a view of the heterogeneous model domain with a Vinton lens placed at the center of an Ottawa sand and concentration contours of PFBS, representing a short-chain PFAS, compared to PFOA, which represents a long-chain PFAS. Fig. 1c shows that higher PFOA concentration was retained in the flow cell compared to PFBS mid-way through the elution, which justifies the mass removal efficiency of the short-chain PFAS. As the mass removal progressed, mass removal of the short-chain PFAS became more efficient in the heterogeneous domain. The inflection points between the concave curve and convex curve occurred at 0.83, 0.78, 0.80, 0.71, and 0.72 MR for PFBS, PFPeA, PFHxS, PFOA, and PFOS, which were consistent with the order of PFAS chain-length from shorter to longer. Later inflection points and lower n1 values (i.e., 1.67, 1.75, 1.68, 1.79, and 2.21, for PFBS, PFPeA, PFHxS, PFOA, and PFOS, respectively) were associated with shorter-chain length indicating a more efficient mass removal. The elution PVs increased in order from PFBS, PFPeA, PFHxS, PFOA, to PFOS (Tables S17–S21). Even though PFOA and PFOS are both C8, PFOS had a higher elution PV, which was a transport delay influenced by the sulfonic acid functional group.

Although the BTCs of the two homogeneous domains showed different transport behaviors among the PFAS, including different peak arrival and elution pore volumes, the MFR/MR curves were less sensitive to the type of PFAS as observed by low n1 variability for all PFAS (Fig. 2). Although both BTCs and MFR/MR curves provide complementary information to assess the effectiveness of remediation methods, BTCs tend to be more suitable to describe the transport behavior and compare the results among different PFAS in homogeneous soils. The elution behavior, which may have relevance for both risk assessment and effectiveness of contaminant remediation, is similar in the homogeneous soils despite the variability of soils hydraulic properties or the PFAS chain-length and functional group.

3.2. Model sensitivity of homogeneous domains

3.2.1. Model sensitivity to homogeneous K_S

In the context of the ADE, K_S results in faster flow velocities, leading to more rapid advection of solutes through the porous domain, earlier contaminant breakthrough at monitoring locations, and faster removal from porous systems (Yeh et al., 2015). In this study, we prescribed a constant flux boundary condition for the entire simulation, which limits the numerical effect of varying the hydraulic conductivity. Fig. 3 shows BTCs and MFR/MR curves for the five PFAS in homogeneous Ottawa sand and homogeneous Vinton using three statistics of K_S values for each soil (i.e., 11.28, 1.26, and 0.14 cm/min for Ottawa sand and 0.63, 0.07, and 0.01 cm/min for Vinton). Table 1 shows the standard deviation of n1 and PV for the three K_d statistics. The effect of the prescribed flux boundary condition limits model sensitivity to K_S as $\sigma_{n1} = 0$ and $\sigma_{PV} = 0$ (Table 1). The range of K_s of natural soils is highly variable between soils and within the same soil compared to other soil hydraulic properties (Camp, 1976; Hitzelberger et al., 2022). Camp (1976) found K_S values ranging from < 0.001 m/d to 0.12 m/d in the same type of soil. Average K_s of Ottawa sand and Vinton are within two orders of magnitude (i.e., 1.26 ± 1.06 cm/min and 0.0702 ± 0.5 cm/min). Hitzelberger et al. (2022) found that a moderate amount of heterogeneity in K_s has created a contaminant sink in the lower permeability zone. This local heterogeneity can create secondary sources and increase the retention of contaminants. Although this work focuses on water-saturated conditions, unsaturated conditions in the vadose zone can include additional parameter variability as well as additional sorption retention processes such as AWIA.

3.2.2. Model sensitivity to homogeneous θ_S

Higher values of θ_S were associated with decreases in pore-water velocity, which delays contaminant arrival and elution even for the water-saturated conditions examined herein. Alternatively, higher θ_S also reduces contaminant retardation (eq. (3), which is expected to accelerate contaminant arrival and increase the contaminant

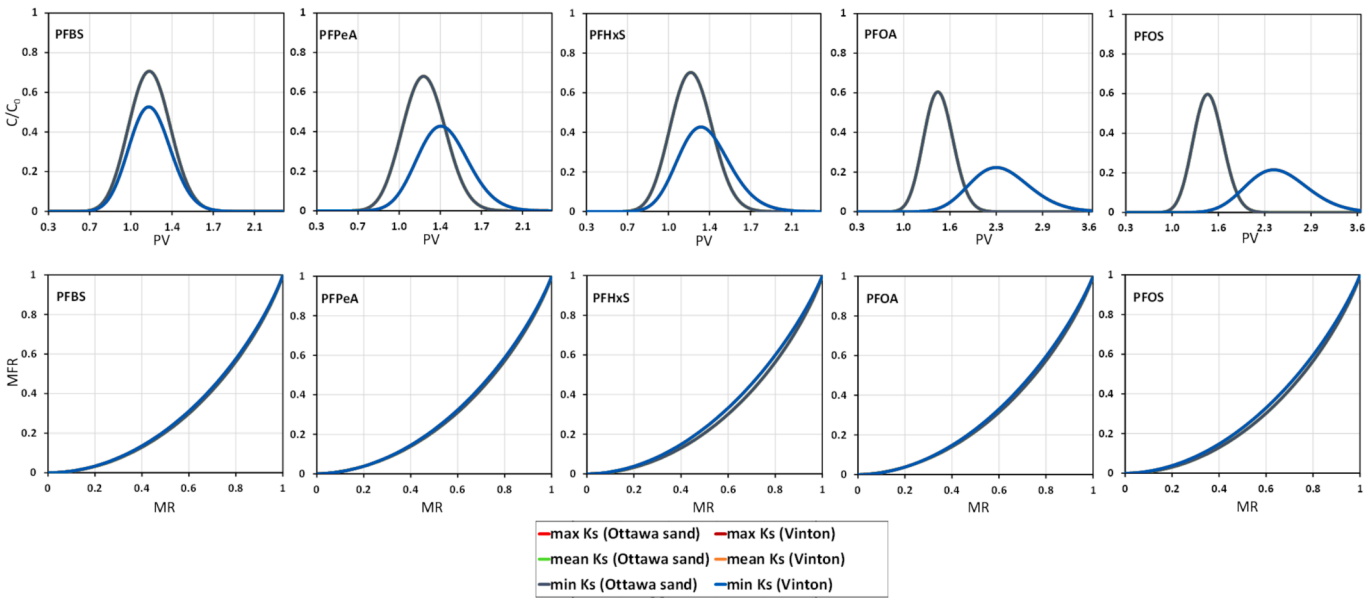

Fig. 3. Comparison of BTCs and MFR/MR curves of the homogeneous domains in Ottawa sand and Vinton using variable saturated hydraulic conductivity values (K_S).

Table 1
Standard deviations of n1 (σ_{n1}), n2 (σ_{n2}), and elution PV (σ_{PV}) for homogeneous and heterogeneous models with variable K_S values.

		Homogeneous Ottawa Sand	Homogeneous Vinton	Heterogeneous
PFBS	σ_{n1}	0.00	0.00	0.28
	σ_{n2}	–	–	0.03
	σ_{PV}	0.00	0.00	33.29
PFPeA	σ_{n1}	0.00	0.00	0.37
	σ_{n2}	–	–	0.02
	σ_{PV}	0.00	0.00	38.33
PFHxS	σ_{n1}	0.00	0.00	0.27
	σ_{n2}	–	–	0.02
	σ_{PV}	0.00	0.00	62.78
PFOA	σ_{n1}	0.00	0.00	0.38
	σ_{n2}	–	–	0.01
	σ_{PV}	0.00	0.00	114.06
PFOS	σ_{n1}	0.00	0.00	0.20
	σ_{n2}	–	–	0.02
	σ_{PV}	0.00	0.00	107.86

breakthrough concentration. Fig. 4 compares BTCs and MFR/MR curves of the five PFAS in homogeneous Ottawa sand and homogeneous Vinton, estimated from models using three θ_S statistics for each soil (i.e., 0.31, 0.294, and 0.278 for Ottawa sand, and 0.417, 0.395, and 0.373 for Vinton). Higher θs values resulted in late arrivals and elution for all PFAS, which are proportion to the PFAS chain-length. We noticed that higher θs resulted in 4–10 % wider BTCs in Vinton and Ottawa sand compared to the lower θs values, which can be attributed to increased lateral dispersion of the plumes (Fig. 4a-4e). Since θs is inversely correlated with the retardation factor (R), it was expected that higher θs will result in reduced R which was expected to result in earlier arrivals and higher breakthrough C/C_0; however, herein higher θs resulted in delayed PFAS arrivals and lower C/C_0 compared to lower θs values (Fig. 4). This trend suggests that the PFAS transport was more controlled by the contaminant lateral dispersion, which increases with the increase of θs, than the effect of the retardation.

The five PFAS had higher BTCs variability in Ottawa sand compared to Vinton, as both σ_n and σ_{PV} were higher in Ottawa sand, which we speculate was due to a numerical effect (Table 2). When solving the ADE equation (Eq. (2), the model divides the equation by R, which is a function of the ratio K_d/θ_S. All PFAS have lower K_d values in Ottawa sand compared to Vinton (Table S3). When the mean K_d value of the PFAS in Ottawa sand is divided by the three different θ_S statistics of Ottawa sand, this yields values (e.g., X1, X2, and X3) with lower mean and standard deviation compared to the values from dividing the average K_d of Vinton by the three different θ_S statistics of Vinton (e.g., Y1, Y2, and Y3). Dividing the ADE equation by these values is equivalent to inverting those values, and therefore the standard deviation of the inverse is approximated by the standard deviation of the values divided by the mean of the values. For example, dividing mean K_d of PFBS in Ottawa sand (2.29E-03 cm^3/g) by the three different θ_S statistics of Ottawa sand (i.e., 0.31, 0.294, and 0.28) yields X1 = 7.36E-3, X2 = 7.77E-3, and X3 = 8.23E-3. Alternatively, dividing mean K_d of PFBS in Vinton (1.37E-2 cm^3/g) by three different θ_S statistics of Vinton (i.e., 0.42, 0.40, and 0.37) yields Y1 = 3.28E-2, Y2 = 3.46E-2, and Y3 = 3.67E-2. Dividing any real positive number by X1, X2, and X3 will yield three values with higher standard deviation than the one we get by dividing the same real positive number by Y1, Y2, and Y3.

The BTCs of the PFBS, PFPeA, and PFHxS aligned very closely in Ottawa sand, as these have comparable mean K_d values in Ottawa sand. However, PFPeA and PFHxS had longer retention, lower BTC C/C_0, and greater elution PVs in Vinton compared to PFBS, as K_d for PFPeA and PFHxS are higher than PFBS in Vinton (Fig. 4). The BTCs of PFOA and PFOS were very comparable in both soils, though, PFOS has a slightly dampened BTC C/C_0 and greater PV elution. The MFR-MR curves for all PFAS had minimal sensitivity to θ_S compared to the BTCs, as σ_n values did not exceed 0.11 and σ_{PV} spanned within a higher range (0.12 – 0.31) (Table 2).

3.2.3. *Model sensitivity to homogeneous K_d*

Contaminant sorption and R is a function of K_d, and increasing R leads to decreased solute advection and dispersion and reduced breakthrough concentration. Fig. 5 compares the BTCs and MFR/MR curves of the five PFAS in Ottawa sand and Vinton, estimated using max, mean, and min K_d statistics for each soil (Table S3). The sensitivity of the BTCs of the homogeneous domains to K_d variability were notably lower compared to the BTCs sensitivity to θ_S, since the BTCs were closely matched together for each PFAS (Fig. 5). The standard deviation of n1 using the three K_d statistics ranged closely between (0.04 – 0.12) in homogeneous Ottawa sand and (0.01 – 0.1) in homogeneous Vinton, which reflects low sensitivity of the MFR/MR curves to K_d variability.

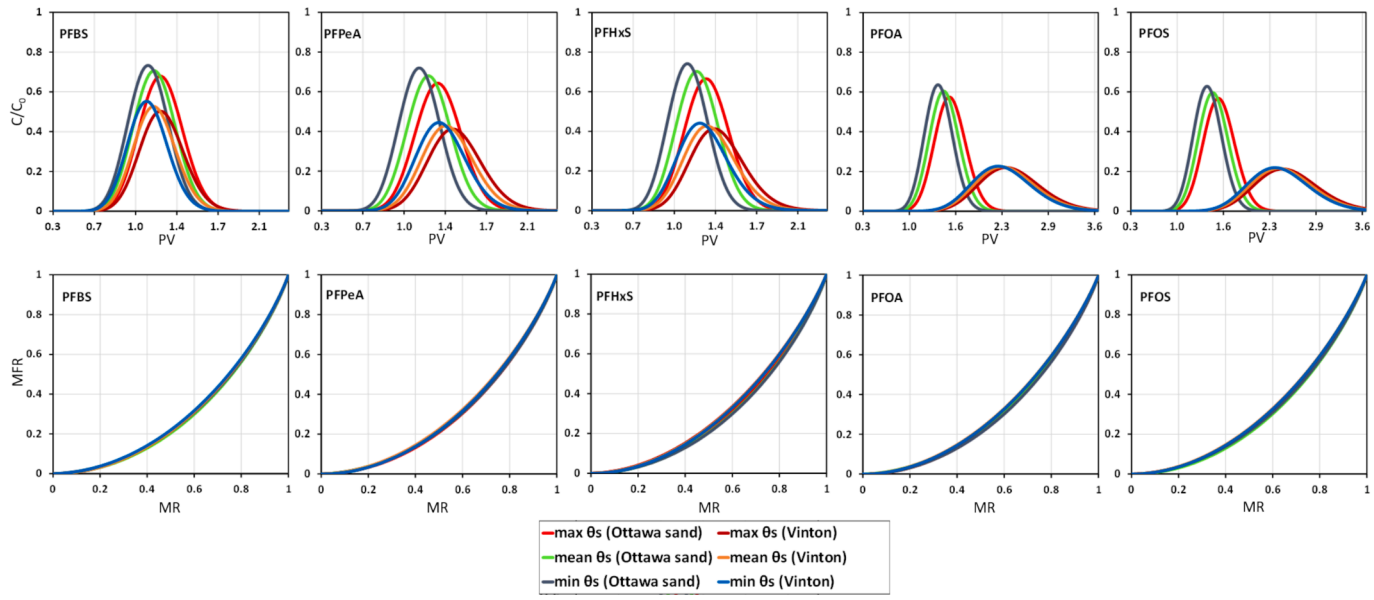

Fig. 4. Comparison of BTCs and MFR/MR curves of the homogeneous domains in Ottawa sand and Vinton using variable porosity values (θ_S).

Table 2
Standard deviations of n1 (σ_{n1}), n2 (σ_{n2}), and elution PV (σ_{PV}) for homogeneous and heterogeneous models with variable θ_S values.

		Homogeneous Ottawa Sand	Homogeneous Vinton	Heterogeneous
PFBS	σ_{n1}	0.08	0.06	0.35
	σ_{n2}	–	–	0.02
	σ_{PV}	0.21	0.20	1.39
PFPeA	σ_{n1}	0.09	0.09	0.38
	σ_{n2}	–	–	0.02
	σ_{PV}	0.31	0.20	1.36
PFHxS	σ_{n1}	0.09	0.08	0.33
	σ_{n2}	–	–	0.01
	σ_{PV}	0.31	0.12	1.56
PFOA	σ_{n1}	0.10	0.05	0.11
	σ_{n2}	–	–	0.01
	σ_{PV}	0.31	0.13	0.24
PFOS	σ_{n1}	0.11	0.05	0.09
	σ_{n2}	–	–	0.01
	σ_{PV}	0.31	0.20	1.65

The standard deviation of PV using three K_d statistics of Ottawa sand ranged between (0.01 – 0.06) for all PFAS, which reflects low BTC sensitivity of these models to K_d. The standard deviation of PV using three K_d statistics of Vinton was also low for the short-chain (ranged 0.03–0.06) compared to the longer-chained PFOA and PFOS (0.25 and 0.26). This concludes that PFOA and PFOS in Vinton were more sensitive to K_d variability than PFOA and PFOS in Ottawa sand and the short-chain PFAS in both soils. The standard deviations of K_d statistics of PFOS and PFOA in homogeneous Vinton were 1.5 and 1.64 cm^3/gm, which were one order of magnitude higher than that in homogeneous Ottawa sand and one order of magnitide higher than the short-chain PFAS in both homogeneous soils. This explains the high sensitivity of PFOS and PFOA elution PV in homogeneous Vinton. Overall, model sensitivity to K_d variability increased with the increase of the span of K_d statistics (i.e., max, mean, and min), which was determined by the span of the coefficients for the Freundlich isotherm (K_f) that was estimated by Zeng et al. (2021) by scaling K_f of PFOS based on the PFAS organic carbon-normalized distribution coefficients (K_{oc}) reported in the literature.

To summarize these findings for homogeneous and water-saturated systems, K_S was amongst the parameters with smaller effect on model sensitivity compared to K_d and θ_S. However, the rank of the most sensitive parameters in unsaturated soils was generally controlled by the relative importance of SPA and AWIA, which depends on the level of unsaturation, PFAS charecteristics, and the applied concentration. The unsaturated models of PFBS and PFPeA as illustrated by Zeng et al. (2021) were more sensitive to the nonlinearity of K_d. The two chemicals had SPA that was comparable with or greater than AWIA. The other long-chain chemicals (i.e., PFOA, PFOS, and PFHxS) had higher AWIA than SPA, and therefore nonlinearity of SPA was negligible (Zeng et al., 2021). For water-saturated media results presented here, where AWIA is not present, model sensitivity to K_d was greater for long-chain chemicals in Vinton. The MFR/MR of the long-chain PFAS were not sensitive to to K_d in either soil.

3.3. Model sensitivity of heterogeneous domain

Inclusion of the less hydraulically accessible Vinton lens within Ottawa sand resulted in development of a preferential flow-path around Vinton, which resulted in accelerated PFAS plume arrival. Vinton has higher K_d values for all five PFAS than Ottawa sand, which resulted in an increased PFAS retention time and increased elution PVs in Vinton. Also, Vinton has higher porosity than Ottawa sand, which was expected to decrease pore-water velocity through the Vinton and PFAS retardation. The behavior of PFAS mixtures further complicates the transport in heterogeneous aquifers where variability in K_S and θ_S results in preferential flow paths. In such environments, MFR/MR curves may exhibit a tailing effect, where short-chain PFAS exhibit rapid breakthrough, while long-chain PFAS show prolonged delays in concentration declines known as tailing. The presence of heterogeneous soils often creates distinct flow zones, with some areas allowing rapid PFAS transport and others retaining contaminants longer, further complicating the shape of the MFR/MR curve (Hitzelberger et al., 2022). Figs. 6-8 compares the BTCs and MFR/MR curves of the heterogeneous domains using nine statistics combinations of each of the three parameter K_S, θ_S, and K_d of Ottawa sand and Vinton, assuming that while one parameter was variable, the other two parameters were at their mean values.

3.3.1. Model sensitivity to heterogeneous K_S

Hydraulic conductivity plays a crucial role in contaminant transport in soils and aquifers (Yeh et al., 2015). Higher K_S allows groundwater to flow more easily, leading to higher efficiency of contaminant removal. Fig. 6 compares the BTCs and MFR/MR curves for the heterogeneous

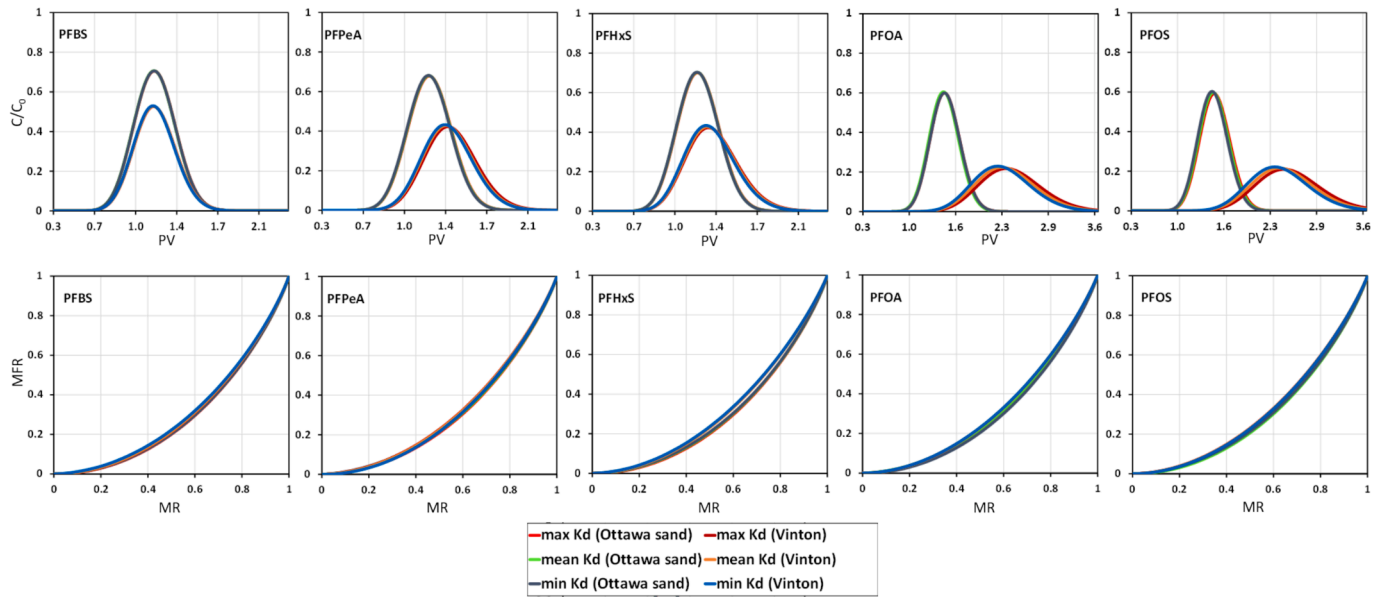

Fig. 5. Comparison of BTCs and MFR/MR curves of the homogeneous domains using Ottawa sand and Vinton using variable solid-phase adsorption coefficients values (K_d).

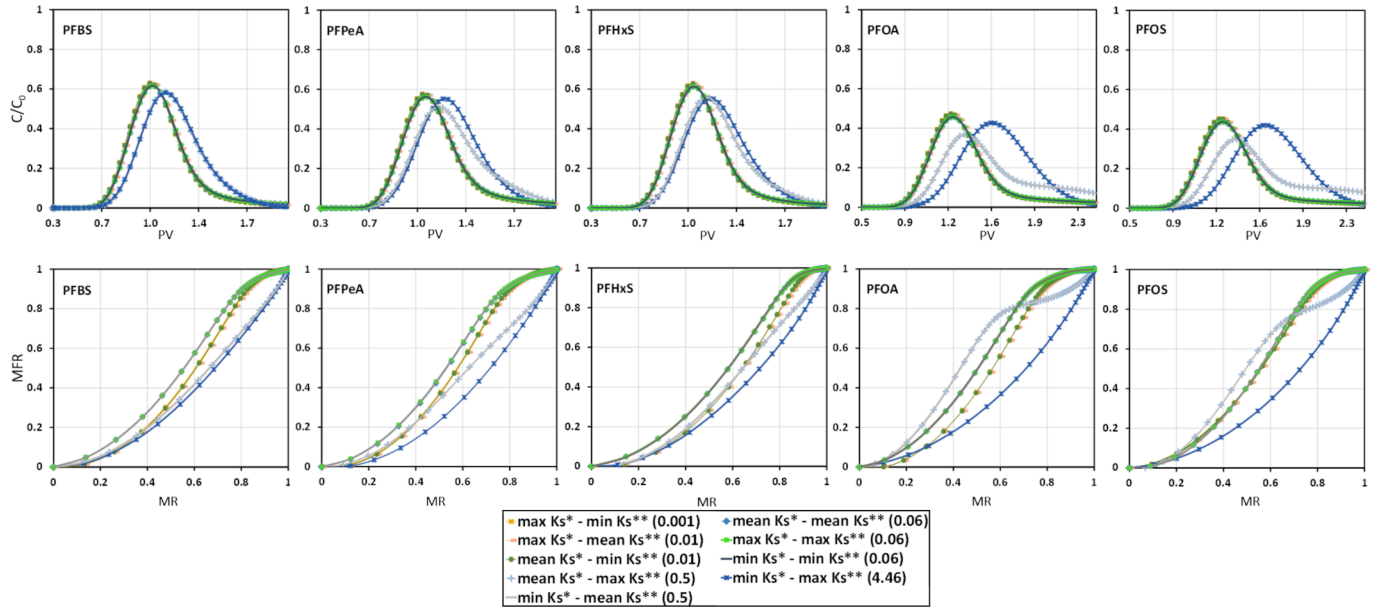

Fig. 6. Comparison of BTCs and MFR/MR curves of the heterogeneous domain using variable saturated hydraulic conductivity (K_S) values. (*) refers to Ottawa sand and (**) refers to Vinton.

domain for the five PFAS using nine statistical combinations of K_S of Ottawa sand and K_S of Vinton, while θ_S and K_d were at their mean values for the two soils. In Fig. 6, K_S of Vinton was referred to as 'K_S**' and K_S of Ottawa sand was referred to as 'K_S*'. We found that the ratios K_S^{**}/K_S^{*} have defined the transport behavior and the shape of the BTCs and MFR/MR curves. The ratio K_S^{**}/K_S^{*} was estimated using nine combinations as follows, $maxK_S^{**}/maxK_S^{*}$, $maxK_S^{**}/meanK_S^{*}$, $maxK_S^{**}/minK_S^{*}$, $minK_S^{**}/maxK_S^{*}$, $meanK_S^{**}/maxK_S^{*}$, $\min K_S^{**}/meanK_S^{*}$, $meanK_S^{**}/meanK_S^{*}$, $meanK_S^{**}/minK_S^{*}$, and $minK_S^{**}/minK_S^{*}$, which yielded the values 0.06, 0.5, 4.46, 0.001, 0.01, 0.01, 0.06, 0.5, and 0.06, respectively. At $maxK_S^{**}/minK_S^{*} = 4.46$, K_S of Vinton is higher than K_S of Ottawa sand, therefore Vinton became more hydraulically accessible than Ottawa sand. This reversed pattern in K_S has led to accelerated contaminant front through Vinton and reduced elution PV compared to the condition where average K_S of Ottawa sand and mean K_S of Vinton were used in the model. Even though K_d of Vinton is higher than K_d of Ottawa sand, the effect of K_S was controlling the transport of PFAS, as PFAS transported faster through Vinton despite the larger K_d values. At the ratio of 4.46, the BTCs followed a bell-shape trend and the MFR-MR curves followed a concave trend, similar to a homogeneous domain. The elution PVs for all PFAS were at their lowest values (i.e., 5.31, 6.7, and 5.88 for PFBS, PFPeA, and PFHxS, respectively), which indicates high efficiency of mass removal. At $K_S^{**}/K_S^{*} = 0.5$, the domain was similar to a homogeneous domain, which was expected as the ratio approaches one. The BTCs of the short-chain PFAS followed a bell-shape trend with minimal tailing, which is generally associated with one mass source zone. This suggests that at $K_S^{**}/K_S^{*} = 0.5$, the effect of K_S heterogeneity for the

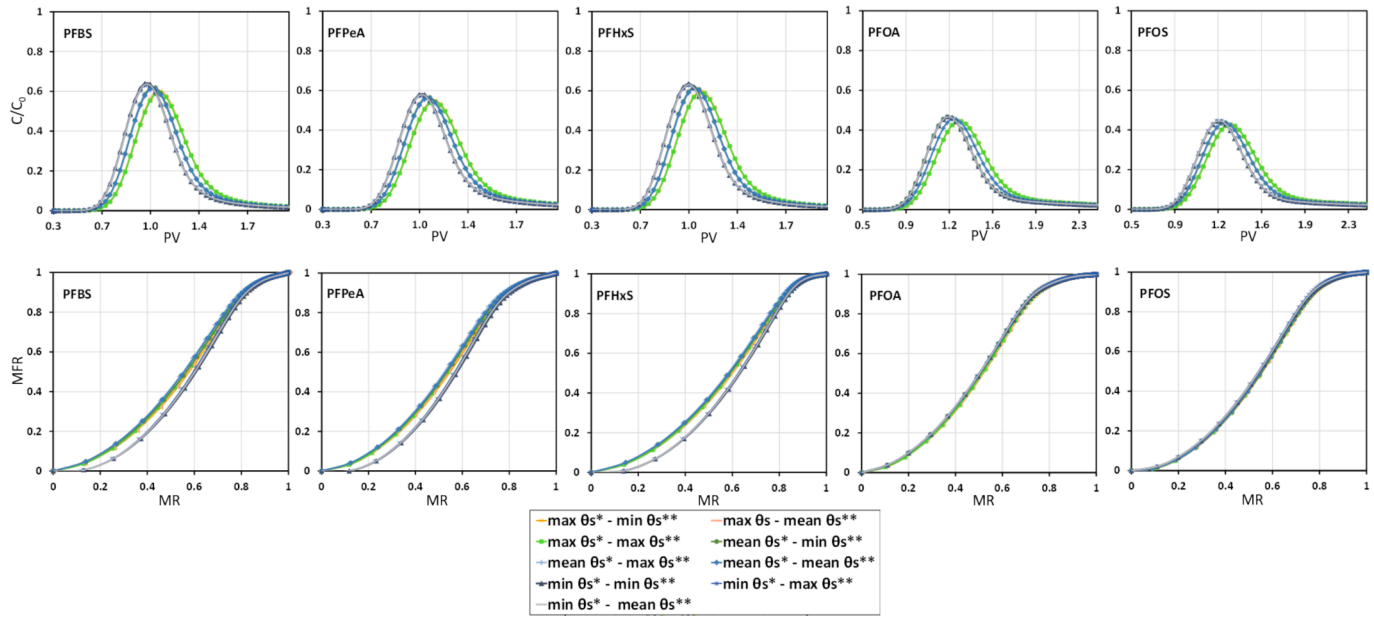

Fig. 7. Comparison of BTCs and MFR/MR curves of the heterogeneous domain using variable porosity (θ_S) values. (*) refers to Ottawa sand and (**) refers to Vinton.

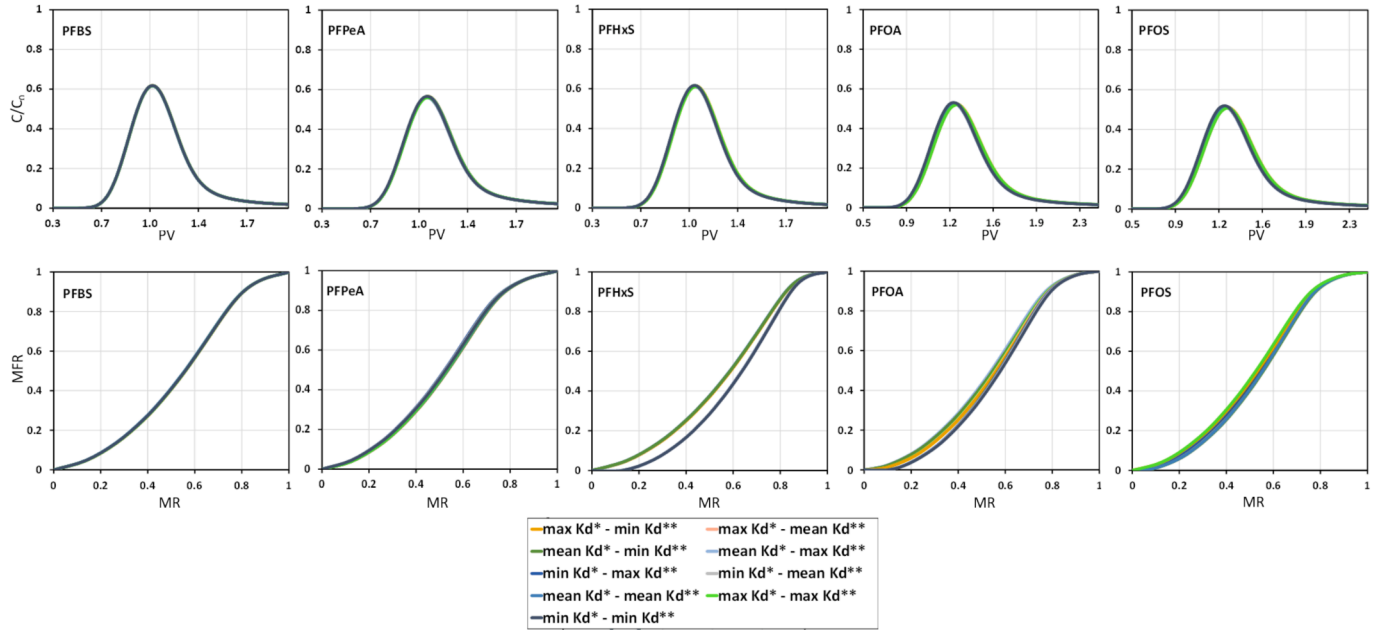

Fig. 8. Comparison of BTCs and MFR/MR curves of the heterogeneous domain using variable solid-phase adsorption coefficients (K_d) values. (*) refers to Ottawa sand and (**) refers to Vinton.

short-chain PFAS was minimal. The MFR/MR curves for models with 0.5 ratio followed a 1:1 straight line, indicating a similar rate of mass flux reduction and contaminant mass removal (Fig. 6). The 0.5 ratio also had lower mass removal efficiency for the short-chain PFAS compared to the ratio 4.46 (or higher mass flux reduction for the same mass removed). This lower mass removal efficiency was reflected in larger elution PVs compared to the 4.46 ratio. The effect of K_d heterogeneity in this case was also negligible, as the higher K_d values of Vinton did not overcome the effect of the minor amount of heterogeneity for K_S, as indicated by the trends of the BTCs and MFR/MR curves described above.

For the two longer-chain PFAS, at $K_S^{**}/K_S^{*} = 4.46$, the BTCs and MFR/MR curves were consistent with the trends of the short-chain PFAS following similar to the homogeneous domain trends (Fig. 6d–j). The elution PVs were at their lowest values (i.e., 7.46 for PFOA and 7.58 for PFOS). At $K_S^{**}/K_S^{*} = 0.5$, the BTCs for the long-chain PFAS were asymmetrical and had a tailing effect reflecting the mass retention at the secondary mass source (Fig. 6d–j). However, the elution PVs were relatively low (13.6 for PFOA and 14.1 for PFOS) compared to the smaller K_S^{**}/K_S^{*} ratios (0.001, 0.01. and 0.06). MFR/MR curves followed a trend close to a straight line at the primary source, which indicates a consistent and constant rate of contaminant removal, followed by an inflection point, and a concave curve at the secondary mass source. The inflection points arrived at lower mass removal than the smaller K_S^{**}/K_S^{*} ratios, which indicates efficient mass removal at the primary source zone. The MFR/MR beyond the inflection points followed a concave curve at the secondary mass source, which indicated efficient removals

from the secondary mass source. This concave trend was not typical for a secondary source zone, and the curve usually followed a convex trend. However, at the ratio 0.5, the secondary mass source was more hydraulically accessible, allowing for a more efficient mass removal.

At smaller ratios (K_S^{**}/K_S^{*} = 0.06, 0.01, and 0.001), the MFR/MR curves followed a concave curve at the primary source zone and a convex curve at the secondary mass zone for both short-chain and long-chain PFAS. At K_S ratios of 0.01 and 0.001, the mass removal from the primary source zone was more efficient compared to a ratio of 0.06 for all PFAS, except for PFOS, which had similar MR efficiency, and that was reflected in higher n1 for the smaller ratios (Fig. S3a). At smaller K_S ratios, contaminants have higher tendency to create preferential flow paths along the high permeability zone, which can potentially result in faster transport and breakthrough and more efficient contaminant removal. However, despite that removal efficiency at the primary source zone, models with smaller K_S ratios had larger elution PVs due to PFAS retention at the secondary source zone (Fig. S3b). In general, elution PVs were consistent with K_S ratios, as larger ratios have resulted in accelerated contaminant removal. At the aquifer scale, this behavior can be reversed if K_S is positively correlated to K_d. In this study, K_d and K_S of Ottawa sand and Vinton are inversely correlated, nevertheless, a positive correlation was observed for weathered crystalline rocks due to increase in the sorption reactive sites and fracture aperture, which results in an increase in both K_d and K_S (Rumynin and Nikulenkov, 2016). In the literature, other exceptions exist where increase of specific sorption sites in the solids had little effect on the K_S both in sedimentary and crystalline rocks (Dai et al., 2009; Zhao et al., 2005). PFAS compounds in mixtures often compete for adsorption sites, which can affect their transport behavior and can result in greater retention in soils, especially in regions with high organic matter or clay content (Brusseau et al., 2019; Gagliano et al., 2020). This can lead to a complex scenario in heterogeneous vadose zones where short-chain PFAS can migrate faster through more permeable layers, while long-chain PFAS are more likely to be retained in finer-textured soils (Brusseau, 2021; Soltanian & Ritzi, 2014).

We noted that the behavior of the BTCs and MFR/MR curves was independent of area-weighted K_S averages summarized in Table S10. For example, the ratios $maxK_S^{**}/maxK_S^{*}$, $meanK_S^{**}/meanK_S^{*}$, and $\min K_S^{**}/minK_S^{*}$ have the same value (0.06), which corresponded to similarity for BTCs and MFR/MR curve results; however, they have distinctively different K_S area-weighted averages (i.e., 60.96, 547.69, and 4903.2). This is largely due to the fact that the linear correlation between K_S ratios and K_S area-weighted average does not have a consistent slope for the entire range of area-weighted K_S averages (Fig. S2). For example, these area-weighted K_S averages (0.127, 0.133, and 0.189), which are within the same order of magnitude, are positively correlated with the K_S ratios (0.06, 0.5, and 4.46), with a correlation slope of 70.88. Whereas, the area-weighted K_S averages (1.135, 1.141, and 1.197), which are one order of magnitude higher than the previous range, are positively correlated with the K_S ratios (0.01, 0.06, and 0.5), with a correlation slope of 7.89. Therefore, the correlation slope decreased significantly with each increase in the range of area-weighted K_S averages. There is also an overlap between the ranges of the K_S ratios correlated with different ranges of area-weighted K_S averages. Regressions between the n1 parameters versus area-weighted K_S averages and between elution PV versus K_S area-weighted averages reflected lack of a consistent pattern and correlation (Fig. S3).

3.3.2. Model sensitivity to heterogeneous θ_S

Fig. 7 compares the BTCs and MFR/MR curves of the heterogeneous domain using nine statistics combinations of θ_S of Ottawa sand (θ_S^{*}) and θ_S of Vinton (θ_S^{**}) while K_S and K_d of the two soils were at their mean values. Similar to the homogeneous domains, lower θ_S area-weighted average resulted in accelerated PFAS concentration arrival and elution and narrow BTC peaks (Fig. 7). The peak of the BTCs decreased as a function of the PFAS chain-length as K_d increased with the chain-length and with sulfonic acid PFAS. The area-weighted averages are affected by the specific area and the parameter statistics of each soil, for example, smaller θ_S area-weighted averages were associated with minimum θ_S of Ottawa sand, which covers a large area (432 cm^2) in the heterogeneous domain (480 cm^2). Using different domain area distributions between the different soils is expected to affect the transport behavior of PFAS and the shapes of the BTCs and MFR/MR curves. The short-chain PFAS had more efficient removals for the three models with lowest θ_S area-weighted averages, which are associated with min θ_S* (i.e., models with min θ_S of Ottawa sand showed more efficient removals, higher n1 values, and earlier inflection points), despite the value of θ_S^{**} (Fig. 7). This minimum area-weighted average θ_S increased pore-water velocity, which explains the high removal efficiency.

The MFR/MR curves of PFOS and PFOA showed less sensitivity to θ_S variability. We attribute this lack of sensitivity to θ_S to the large K_d of PFOA and PFOS, which controls their retention and transport behavior. Regressions between n1 versus θ_S area-weighted average and n1 versus θ_S ratios indicate lack of trend (Fig. S5a and b). The regressions between elution PVs versus θ_S area-weighted average and elution PVs versus θ_S ratios show linear correlations that are defined by the statistical combinations between θ_S* and θ_S^{**}(Fig. S5c and d). For example, the elution PVs versus θ_S area-weighted average had the smallest intercept for the three combinations including max θ_S* with min θ_S^{**}, mean θ_S^{**}, and max θ_S^{**}, while the combinations with min θ_S* had the largest intercept (Fig. S5c). While the elution PVs versus θ_S ratios had the largest intercept for the three combinations including max θ_S* with min θ_S*, mean θ_S*, and max θ_S*, and the combinations with min θ_S* had the smallest intercept (Fig. S5d). Also, the correlations between the elution PVs versus θ_S ratios overlap between the different combinations. The previous trends are specific for the types of soils used in this investigation and can vary with other soils. It was also observed that at combinations with max θ_S^{**} required higher elution PVs to achieve zero C/C_0, even for a smaller weighted average θ_S value, which combines max θ_S^{**} and min θ_S* (Tables S17–S21). Efficient mass removal at the primary source is mainly controlled by the porosity of the high permeability zone, but that does not insure an efficient contaminant mass removal from the entire heterogeneous domain. Mass removal is also controlled by the porosity of the low permeability zone, and minimum θ_S will result in less PV to remove the contaminant from the domain. The weighted average of θ_S defines the peak arrival; however, K_d of the lower K_s zone defines the complete elution of the contaminant.

3.3.3. Model sensitivity to heterogeneous K_d

Soil chemical heterogeneity due to variable grain size, mineral composition, and organic matter content influences kinetic and solid-phase adsorption and manifests into nonideal transport behavior including low concentration tailing. Therefore, it is expected that K_d area-weighted average influences the net rate of contaminant retention and remediation within geochemically heterogeneous soils. Fig. 8 compares the BTCs and MFR/MR curves of the heterogeneous domain using nine statistical combinations of K_d of Ottawa sand (K_d^{**}) and K_d of Vinton (K_d^{*}), while θ_S and K_S of the two soils were at their mean values. Table 3 shows the standard deviations of n1, n2, and elution PV for each PFAS created from models with variable K_d statistics. Fig. S6a–e show regressions between n1 parameters and K_d area-weighted averages. Also, Fig. S7a–e show regressions between n1 parameters and K_d ratios, and all the figures did not indicate consistent patterns or correlations. This reflects the low sensitivity of the MFR/MR curves at the primary source zone (which is associated with n1) to K_d variability as K_d were similar and less variable for all PFAS in Ottawa sand. The secondary source zone (which is associated with n2) was also insensitive to K_d variability within the same PFAS, as indicated by low σ_{n2} values (Table 3). However, average n2 increased following the PFAS chain-length changes as follows (average n2 = 0.35, 0.34, 0.26, 0.24, 0.23

Table 3
Standard deviations of n1 (σ_{n1}), n2 (σ_{n2}), and elution PV (σ_{PV}) for homogeneous and heterogeneous models with variable K_d values.

		Homogeneous Ottawa Sand	Homogeneous Vinton	Heterogeneous
PFBS	σ_{n1}	0.04	0.08	0.01
	σ_{n2}	–	–	0.00
	σ_{PV}	0.01	0.03	0.08
PFPeA	σ_{n1}	0.06	0.10	0.04
	σ_{n2}	–	–	0.01
	σ_{PV}	0.01	0.07	0.37
PFHxS	σ_{n1}	0.08	0.02	0.41
	σ_{n2}	–	–	0.02
	σ_{PV}	0.01	0.06	0.30
PFOA	σ_{n1}	0.12	0.01	0.29
	σ_{n2}	–	–	0.01
	σ_{PV}	0.05	0.25	1.68
PFOS	σ_{n1}	0.08	0.04	0.22
	σ_{n2}	–	–	0.01
	σ_{PV}	0.06	0.26	1.84

for PFBS, PFPeA, PFHxS, PFOA, PFOS, respectively) (Tables S21–S25). Higher n2 values indicate more efficient removal from the secondary source zone. The elution PV was positively correlated with both K_d area-weighted averages and K_d ratios (Fig. S6f–j and S7F–j). We found that K_d area-weighted averages were positively correlated to K_d ratios, however, the intercept of the linear correlation changed based on the statistics of Ottawa sand. For example, the three statistical combinations with max K_d* (i.e., max K_d*/max K_d^{**}, max K_d*/mean K_d^{**}, and max K_d*/min K_d^{**}) had a higher intercept value, followed by the three statistics combinations with mean K_d* and then the three statistics combinations with min K_d*. Elution PVs were consistent with the trends of PFAS chain-length, which increased following this order PFBS, PFPeA, PFHxS, PFOA, and PFOS.

4. Conclusions

This modeling sensitivity analysis has assessed variability and controls over PFAS transport behavior through evaluation of both BTCs and MFR versus MR of five common PFAS contaminants that have different carbon–fluorine chain length and two functional groups in homogeneous and heterogeneous (two domain) water-saturated subsurface systems. The results reveal:

1. MFR/MR curves are more sensitive to fluid flow parameter variability than BTCs, making them more suitable for detailed assessments of solute transport in heterogeneous environments.
2. In heterogeneous soils, the ratio of saturated hydraulic conductivity between different soil types significantly influences the BTC behavior, the slope of log MFR versus MR (n1), and the timing of inflection points.
3. The model's sensitivity to variations in soil water content (θ_S) is higher for short-chain PFAS. In contrast, the substantial distribution coefficient (K_d) of long-chain PFAS constrains the sensitivity to changes in θ_S.
4. Models with the lowest θ_S area-weighted averages demonstrate higher mass removal efficiencies for short-chain PFAS. Conversely, the removal efficiencies for long-chain PFAS remain relatively unaffected by θ_S variability.
5. Regardless of variations in soil hydraulic properties or PFAS chain length and functional group, the effectiveness of remediation remains consistent in homogeneous soil environments.

Long-chain PFAS tended to adsorb more strongly to soil particles, resulting in concentration tailing and delayed transport in lower-permeability zones, while short-chain PFAS moved more rapidly through higher-permeability zones (Guo et al., 2020; Silva et al., 2021; Brusseau et al. 2019). MFR/MR results were consistent with the findings of Hitzelberger et al. (2022) that MFR was higher in lower-permeability layers, due to increased contaminant retention, whereas in higher-permeability zones had lower MFR but higher MR. These findings underscored the critical role of subsurface parameter structure, or architecture, in influencing the effectiveness of PFAS risk analysis and contaminant remediation strategies, particularly in complex, heterogeneous environments. For situations where addressing the source zone is important, for example when the goal of risk assessment or remediation is to prevent contaminant plumes from spreading to sensitive receptors, using MFR/MR curve is crucial. Regulatory agencies have more recently been setting standards not only for concentrations but also for the overall reduction in mass flux. Demonstrating effective MFR and MR aligns with regulatory expectations for successful aquifer remediation. The emphasis on MRF and MR is driven by the need to address persistent source zones, manage aqueous contaminant plumes, and reduce the risk of contaminant migration to protect groundwater quality and sensitive receptors from exposure.

CRediT authorship contribution statement

Ruba A.M. Mohamed: Writing – original draft, Visualization, Validation, Methodology, Investigation, Formal analysis. **Mohamad R. Soltanian:** Writing – review & editing, Methodology, Investigation. **Dengjun Wang:** Writing – review & editing, Methodology, Investigation. **Kenneth C. Carroll:** Writing – review & editing, Validation, Supervision, Resources, Project administration, Methodology, Investigation, Funding acquisition, Conceptualization.

Declaration of competing interest

The authors declare that they have no known competing financial interests or personal relationships that could have appeared to influence the work reported in this paper.

Acknowledgments

We appreciate funding support through the Directed Research and Development University Partnerships Supplemental Project Number 233084 from Sandia National Laboratories Laboratory, and we appreciate the support of Sandia National Lab staff including Andrew Knight, Ryan Davis, Mohammad Shohel, Jessica Nicole Kruichak-Duhigg, and Mark J. Rigali. Additional support was provided by the NSF (Award Number (FAIN): 2142686), and this research was supported in part by the intramural research program of the U.S. Department of Agriculture, National Institute of Food and Agriculture, Hatch Project 7006726. We appreciate assistance of Dawn VanLeeuwen and the NMSU ACES Agricultural Statistical Consulting Center (ASCC).

Appendix A. Supplementary data

Supplementary data to this article can be found online at https://doi.org/10.1016/j.jhydrol.2024.132268.

Data availability

Data will be made available on request.

References

Ahrens, L., et al., 2010. Distribution of polyfluoroalkyl compounds in water, suspended particulate matter and sediment from Tokyo Bay. Japan. Chemosphere 79 (3), 266–272.
Akyol, N.H., Demiray, Z., Copty, N.K., Acılıoğlu, T., Akyol, G., 2023. Mass-flux reduction and mass removal relationships (MFR-MR) of pool-dominated multicomponent DNAPLs in a heterogeneous geological system. Global NEST J. 25 (4), 43–55.

Allen-King, R.M., et al., 2015. Hydrophobic organic contaminant transport property heterogeneity in the B orden A quifer. Water Resour. Res. 51 (3), 1723–1743.
Allen-King, R.M., Halket, R.M., Gaylord, D.R., Robin, M.J.L., 1998. Characterizing the heterogeneity and correlation of perchloroethene sorption and hydraulic conductivity using a facies-based approach. Water Resour. Res. 34 (3), 385–396.
Bolan, N., et al., 2021. Remediation of poly-and perfluoroalkyl substances (PFAS) contaminated soils–to mobilize or to immobilize or to degrade? J. Hazard. Mater. 401, 123892.
Brusseau, M.L., et al., 2011. Impact of In Situ Chemical Oxidation on Contaminant Mass Discharge: Linking Source-Zone and Plume-Scale Characterizations of Remediation Performance. Environ. Sci. Tech. 45 (12), 5352–5358.
Brusseau, M.L., 2019. The influence of molecular structure on the adsorption of PFAS to fluid-fluid interfaces: Using QSPR to predict interfacial adsorption coefficients. Water Res. 152, 148–158.
Brusseau, M.L., et al., 2019a. Nonideal Transport and Extended Elution Tailing of PFOS in Soil. Environ. Sci. Tech. 53 (18), 10654–10664.
Brusseau, M.L., et al., 2019b. Comprehensive retention model for PFAS transport in subsurface systems. Water Res. 148, 41–50.
Brusseau, M.L., 2020. Simulating PFAS transport influenced by rate-limited multi-process retention. Water Res. 168.
Brusseau, M.L., 2021. Examining the robustness and concentration dependency of PFAS air-water and NAPL-water interfacial adsorption coefficients. Water Res. 190, 11.
Brusseau, M.L., 2023. Differential Sorption of Short-Chain versus Long-Chain Anionic Per-and Poly-Fluoroalkyl Substances by Soils. Environments 10 (10), 2076–3298.
Camp, C.R., 1976. Determination of hydraulic conductivity for a Louisiana alluvial soil. ASAE St. Joseph, Missouri 49085, 104–108.
Cara, B., Lies, T., Thimo, G., Robin, L., Lieven, B., 2022. Bioaccumulation and trophic transfer of perfluorinated alkyl substances (PFAS) in marine biota from the Belgian North Sea: Distribution and human health risk implications. Environ. Pollut. 311, 119907.
Chen, W., et al., 2023. Impact of reactive mineral facies distributions on radionuclide sorption properties in multiscale heterogeneous granite rocks. Hydrgeol. J. 31 (6), 1581–1597.
Costanza, J., Arshadi, M., Abriola, L.M., Pennell, K.D., 2019. Accumulation of PFOA and PFOS at the Air-Water Interface. Environ Sci Tech Let 6 (8), 487–491.
Cox, C., 2005. Delta method. Encyclopedia of Biostatistics 2.
Cvetkovic, V., Dagan, G., 1994. Transport of kinetically sorbing solute by steady random velocity in heterogeneous porous formations. J. Fluid Mech. 265, 189–215.
Cvetkovic, V.D., Shapiro, A.M., 1990. Mass arrival of sorptive solute in heterogeneous porous media. Water Resour. Res. 26 (9), 2057–2067.
Dagan, G., 1984. Solute transport in heterogeneous porous formations. J. Fluid Mech. 145, 151–177.
Dai, Z., et al., 2012. Identification of sorption processes and parameters for radionuclide transport in fractured rock. J. Hydrol. 414, 220–230.
Dai, Z., Wolfsberg, A., Lu, Z., Deng, H., 2009. Scale dependence of sorption coefficients for contaminant transport in saturated fractured rock. Geophys. Res. Lett. 36 (1).
Dasu, K., Xia, X., Siriwardena, D., Klupinski, T.P., Seay, B., 2022. Concentration profiles of per-and polyfluoroalkyl substances in major sources to the environment. J. Environ. Manage. 301, 113879.
Difilippo, E.L., Brusseau, M.L., 2008. Relationship between mass-flux reduction and source-zone mass removal: analysis of field data. J. Contam. Hydrol. 98 (1–2), 22–35.
DiFilippo, E.L., Brusseau, M.L., 2011a. Application of Light Reflection Visualization for Measuring Organic-Liquid Saturation for Two-Phase Systems in Two-Dimensional Flow Cells. Environ. Eng. Sci. 28 (11), 803–809.
DiFilippo, E.L., Brusseau, M.L., 2011b. Assessment of a simple function to evaluate the relationship between mass flux reduction and mass removal for organic-liquid contaminated source zones. J. Contam. Hydrol. 123 (3–4), 104–113.
DiFilippo, E.L., Carroll, K.C., Brusseau, M.L., 2010. Impact of organic-liquid distribution and flow-field heterogeneity on reductions in mass flux. J. Contam. Hydrol. 115 (1–4), 14–25.
Fabregat-Palau, J., Vidal, M., Rigol, A., 2021. Modelling the sorption behaviour of perfluoroalkyl carboxylates and perfluoroalkane sulfonates in soils. Sci Total Environ 801, 149343.
Gagliano, E., Sgroi, M., Falciglia, P.P., Vagliasindi, F.G.A., Roccaro, P., 2020. Removal of poly- and perfluoroalkyl substances (PFAS) from water by adsorption: Role of PFAS chain length, effect of organic matter and challenges in adsorbent regeneration. Water Res. 171.
Ghisi, R., Vamerali, T., Manzetti, S., 2019. Accumulation of perfluorinated alkyl substances (PFAS) in agricultural plants: A review. Environ. Res. 169, 326–341.
Glüge, J., et al., 2020. An overview of the uses of per-and polyfluoroalkyl substances (PFAS). Environ. Sci. Processes Impacts 22 (12), 2345–2373.
Goltz, M.N., Kim, S., Yoon, H., Park, J., 2007. Review of Groundwater Contaminant Mass Flux Measurement. Environ. Eng. Res. 12, 176–193.
Guelfo, J.L., Higgins, C.P., 2013. Subsurface Transport Potential of Perfluoroalkyl Acids at Aqueous Film-Forming Foam (AFFF)-Impacted Sites. Environ. Sci. Tech. 47 (9), 4164–4171.
B. Guo M.L. Brusseau Challenges and opportunities for porous media research to address PFAS groundwater contamination InterPore Journal 1 2 2024 ipj240824-2.
Guo, B., Zeng, J., Brusseau, M.L., 2020. A Mathematical Model for the Release, Transport, and Retention of Per-and Polyfluoroalkyl Substances (PFAS) in the Vadose Zone. Water Resour. Res. 56 (2), e2019WR026667.
Higgins, C.P., Luthy, R.G., 2006. Sorption of perfluorinated surfactants on sediments. Environ. Sci. Tech. 40 (23), 7251–7256.
Hitzelberger, M., Khan, N.A., Mohamed, R.A.M., Brusseau, M.L., Carroll, K.C., 2022. PFOS Mass Flux Reduction/Mass Removal: Impacts of a Lower- Permeability Sand Lens within Otherwise Homogeneous Systems. Environ. Sci. Tech. 56 (19), 13675–13685.
Hu, X.C., et al., 2016. Detection of poly-and perfluoroalkyl substances (PFASs) in US drinking water linked to industrial sites, military fire training areas, and wastewater treatment plants. Environ Sci Tech Let 3 (10), 344–350.
Huang, D.D., Khan, N.A., Wang, G.C., Carroll, K.C., Brusseau, M.L., 2022. The Co-Transport of PFAS and Cr(VI) in porous media. Chemosphere 286, 7.
Jawitz, J.W., et al., 2008. Laboratory investigation of flux reduction from dense non-aqueous phase liquid (DNAPL) partial source zone remediation by enhanced dissolution. J. Contam. Hydrol. 102 (1–2), 17–28.
Johnson, G.R., Brusseau, M.L., Carroll, K.C., Tick, G.R., Duncan, C.M., 2022. Global distributions, source-type dependencies, and concentration ranges of per- and polyfluoroalkyl substances in groundwater. Sci Total Environ 841 (1), 156602.
Karagunduz, A., Young, M.H., Pennell, K.D., 2015. Influence of surfactants on unsaturated water flow and solute transport. Water Resour. Res. 51 (4), 1977–1988.
Kookana, R.S., Navarro, D.A., Kabiri, S., McLaughlin, M.J., 2022. Key properties governing sorption–desorption behaviour of poly-and perfluoroalkyl substances in saturated and unsaturated soils: a review. Soil. Research.
Kurwadkar, S., et al., 2022. Per-and polyfluoroalkyl substances in water and wastewater: A critical review of their global occurrence and distribution. Sci Total Environ 809, 151003.
Lemke, L.D., Abriola, L.M., Lang, J.R., 2004. Influence of hydraulic property correlation on predicted dense nonaqueous phase liquid source zone architecture, mass recovery and contaminant flux. Water Resour. Res. 40 (12), -.
Li, P., McGarr, J.T., Moeini, F., Dai, Z., Soltanian, M.R., 2024. Sensitivity Analysis and Uncertainty Quantification of PFAS Fate and Transport in Heterogeneous Riparian Sediments. ACS Earth Space Chem. 8 (8), 1560–1573.
Maghrebi, M., et al., 2015. Contaminant tailing in highly heterogeneous porous formations: sensitivity on model selection and material properties. J. Hydrol. 531, 149–160.
Makselon, J., 2019. Binding of per-and polyfluoroalkyl substances (PFASs) to organic soil horizons of peat and more.
Marble, J.C., et al., 2014. Application of a Persistent Dissolved-Phase Reactive Treatment Zone for Mitigation of Mass Discharge from Sources Located in Lower-Permeability Sediments. Water Air Soil Pollut. 225 (11).
Marble, J.C., DiFilippo, E.L., Zhang, Z., Tick, G.R., Brusseau, M.L., 2008. Application of a lumped-process mathematical model to dissolution of non-uniformly distributed immiscible liquid in heterogeneous porous media. J. Contam. Hydrol. 100 (1–2), 1–10.
Mateas, D.J., Tick, G.R., Carroll, K.C., 2017. In situ stabilization of NAPL contaminant source-zones as a remediation technique to reduce mass discharge and flux to groundwater. J. Contam. Hydrol. 204, 40–56.
McGarr, J.T., Mbonimpa, E.G., McAvoy, D.C., Soltanian, M.R., 2023. Fate and Transport of Per-and Polyfluoroalkyl Substances (PFAS) at Aqueous Film Forming Foam (AFFF) Discharge Sites: A Review. Soil Systems 7 (2), 53.
Michael, H.A., Khan, M.R., 2016. Impacts of physical and chemical aquifer heterogeneity on basin-scale solute transport: Vulnerability of deep groundwater to arsenic contamination in Bangladesh. Adv. Water Resour. 98, 147–158.
Nguyen, T.M.H., et al., 2020. Influences of chemical properties, soil properties, and solution pH on soil–water partitioning coefficients of per-and polyfluoroalkyl substances (PFASs). Environ. Sci. Tech. 54 (24), 15883–15892.
Pereira, H.C., Ullberg, M., Kleja, D.B., Gustafsson, J.P., Ahrens, L., 2018. Sorption of perfluoroalkyl substances (PFASs) to an organic soil horizon–Effect of cation composition and pH. Chemosphere 207, 183–191.
Peritore, A.F., Gugliandolo, E., Cuzzocrea, S., Crupi, R., Britti, D., 2023. Current Review of Increasing Animal Health Threat of Per-and Polyfluoroalkyl Substances (PFAS): Harms, Limitations, and Alternatives to Manage Their Toxicity. Int. J. Mol. Sci. 24 (14), 11707.
Rumynin, V.G., Nikulenkov, A.M., 2016. Geological and physicochemical controls of the spatial distribution of partition coefficients for radionuclides (Sr-90, Cs-137, Co-60, Pu-239,240 and Am-241) at a site of nuclear reactors and radioactive waste disposal (St. Petersburg region, Russian Federation). J. Environ. Radioact. 162, 205–218.
Russo, D., Bouton, M., 1992. Statistical analysis of spatial variability in unsaturated flow parameters. Water Resour. Res. 28 (7), 1911–1925.
Schaefer, C.E., et al., 2019. Measurement of aqueous diffusivities for perfluoroalkyl acids. J. Environ. Eng. 145 (11), 06019006.
Sharifan, H., et al., 2021. Fate and transport of per-and polyfluoroalkyl substances (PFASs) in the vadose zone. Sci Total Environ 771, 145427.
Silva, J.A.K., Simunek, J., McCray, J.E., 2020. A Modified HYDRUS Model for Simulating PFAS Transport in the Vadose Zone. Water 12 (10).
Silva, J.A.K., Martin, W.A., McCray, J.E., 2021. Air-water interfacial adsorption coefficients for PFAS when present as a multi-component mixture. J. Contam. Hydrol. 236, 103731.
Šimůnek, J., Šejna, M., Genuchten, M.T.v., 2014. HYDRUS (2D/3D). Software Package for Simulating Two-and Three-Dimensional Movement of Water, Heat, and Multiple Solutes in Variably-Saturated Media, User Manual, Version, 1: 203.
Šimůnek, J., Van Genuchten, M.T., Šejna, M., 2016. Recent developments and applications of the HYDRUS computer software packages. Vadose Zone J. 15 (7).
Slavic, D.R., 2014. Enhanced-solubilization of multicomponent dense immiscible liquid in homogeneous porous media. The University of Alabama.
Soga, K., Page, J.W.E., Illangasekare, T.H., 2004. A review of NAPL source zone remediation efficiency and the mass flux approach. J. Hazard. Mater. 110 (1–3), 13–27.
Soga, K., Page, J.W.E., Illangasekare, T., 2007. The significance of heterogeneity on mass flux from DNAPL source zones: An experimental investigation. J. Contam. Hydrol. 94 (3–4), 215–234.

Soltanian, M.R., Ritzi, R.W., 2014. A new method for analysis of variance of the hydraulic and reactive attributes of aquifers as linked to hierarchical and multiscaled sedimentary architecture. Water Resour. Res. 50 (12), 9766–9776.
Soltanian, M.R., Ritzi, R.W., Dai, Z., Huang, C.C., 2015a. Reactive solute transport in physically and chemically heterogeneous porous media with multimodal reactive mineral facies: The Lagrangian approach. Chemosphere 122, 235–244.
Soltanian, M.R., Ritzi, R.W., Huang, C.C., Dai, Z., 2015b. Relating reactive solute transport to hierarchical and multiscale sedimentary architecture in a L agrangian-based transport model: 1. Time-dependent effective retardation factor. Water Resour. Res. 51 (3), 1586–1600.
Soltanian, M.R., Ritzi, R.W., Huang, C.C., Dai, Z., 2015c. Relating reactive solute transport to hierarchical and multiscale sedimentary architecture in a L agrangian-based transport model: 2. Particle Displacement Variance. Water Resources Research 51 (3), 1601–1618.
Talon, L., Ollivier-Triquet, E., Dentz, M., Bauer, D., 2023. Transient dispersion regimes in heterogeneous porous media: On the impact of spatial heterogeneity in permeability and exchange kinetics in mobile–immobile transport. Adv. Water Resour. 174, 104425.
Teunen, L., Bervoets, L., Belpaire, C., De Jonge, M., Groffen, T., 2021. PFAS accumulation in indigenous and translocated aquatic organisms from Belgium, with translation to human and ecological health risk. Environ. Sci. Eur. 33, 1–19.
Tompson, A.F.B., 1993. Numerical simulation of chemical migration in physically and chemically heterogeneous porous media. Water Resour. Res. 29 (11), 3709–3726.
Van der Zee, S., Van Riemsdijk, W.H., 1987. Transport of reactive solute in spatially variable soil systems. Water Resour. Res. 23 (11), 2059–2069.
Van Glubt, S., et al., 2021. Column versus batch methods for measuring PFOS and PFOA sorption to geomedia. Environ. Pollut. 268, 115917.
Vorst, K.L., Saab, N., Silva, P., Curtzwiler, G., Steketee, A., 2021. Risk assessment of per- and polyfluoroalkyl substances (PFAS) in food: Symposium proceedings. Trends Food Sci. Technol. 116, 1203–1211.
Wang, Y., Khan, N., Huang, D., Carroll, K.C., Brusseau, M.L., 2021a. Transport of PFOS in aquifer sediment: Transport behavior and a distributed-sorption model. Sci Total Environ 779, 146444.
Wang, Y.K., Khan, N., Huang, D.D., Carroll, K.C., Brusseau, M.L., 2021b. Transport of PFOS in aquifer sediment: Transport behavior and a distributed-sorption model. Sci Total Environ 779, 8.
Yeh, T.-C., Khaleel, R., Carroll, K.C., 2015. Flow through heterogeneous geologic media. Cambridge University Press.
Zareitalabad, P., Siemens, J., Hamer, M., Amelung, W., 2013. Perfluorooctanoic acid (PFOA) and perfluorooctanesulfonic acid (PFOS) in surface waters, sediments, soils and wastewater - A review on concentrations and distribution coefficients. Chemosphere 91 (6), 725–732.
Zeng, J., Brusseau, M.L., Guo, B., 2021. Model validation and analyses of parameter sensitivity and uncertainty for modeling long-term retention and leaching of PFAS in the vadose zone. J. Hydrol. 127172.
Zeng, J., Guo, B., 2021. Multidimensional simulation of PFAS transport and leaching in the vadose zone: Impact of surfactant-induced flow and subsurface heterogeneities. Adv. Water Resour. 155, 104015.
Zhao, X., Wallace, R.B., Hyndman, D.W., Dybas, M.J., Voice, T.C., 2005. Heterogeneity of chlorinated hydrocarbon sorption properties in a sandy aquifer. J. Contam. Hydrol. 78 (4), 327–342.